A Cable-Free Digital Sensor-Bus for Structural Health Monitoring of Large Area Composite Structures

Seth S. Kessler[1], Christopher T. Dunn[2], Michael Borgen[3], Ajay Raghavan[4], Jeffrey Duce[5] and David L. Banks[6]

[1,2,3, 4] *Metis Design Corporation, Cambridge, MA, 02141, USA*
skessler@metisdesign.com
cdunn@metisdesign.com
mborgen@metisdesign.com
ajay@metisdesign.com

[5,6] *The Boeing Corporation, Seattle, WA, 98124, USA*
jeff.duce@boeing.com
david.l.banks@boeing.com

ABSTRACT

The integration of structural health monitoring (SHM) systems into in-service applications has been hindered by the implied infrastructure, specifically wires for power and data from each sensor an acquisition unit. Point-of-measurement datalogging can greatly reducing the required quantity of cable by locally converting analog signals into digital data that can be placed on a common sensor-bus. During the present research, this efficient architecture is further enhanced by exploiting direct-write (DW) technologies to produce a cable-free digital sensor-bus. This concept has broad implications particularly for large area composite structures, where significant weight reductions can be achieved.

The present work aims to extend the DW portfolio beyond analog applications to include digital communication. In order to achieve this goal, research was conducted in several areas including ensuring compatibility with existing practical SHM hardware and methods, as well as the optimization of geometric and electrical parameters. Finally, a proof-of-concept experiment has been designed to demonstrate the integration of all the described system elements to detect and localize damage on a composite plate.[*]

1 INTRODUCTION

Implementing structural health monitoring (SHM) can improve asset reliability, safety and readiness while reducing life-cycle costs. However, these advantages come at the expense of weight, power consumption and computational bandwidth. While several viable SHM concepts have been demonstrated in laboratory settings, scaling these systems for large area coverage has presented challenges. Traditional methods require at least 1 analog cable (typically coaxial) from each sensing element to a remote hardware location. Cable runs can become long, introducing EMI susceptibility and signal attenuation due to stray capacitance. Furthermore, this instrumentation can also add > 6 kg/m^2, and introduce failure points due to both environmental and mechanical durability issues.

To mitigate these problems, one technique demonstrated by the present investigators is the use of local sensor digitization. By converting analog signals into digital data at the point-of-measurement, the problems of EMI and attenuation virtually disappear, and a digital sensor-bus can be used to serially connect sensors to minimize total cable length. The use of a digital sensor-bus alone may not be sufficient; there will still be a cable harness to manually install, and durability may still be of concern. Once digitized locally wireless transmission of data becomes an attractive option, however upon closer examination, these methods become infeasible for most applications because of power requirements and regulatory issues. Thus the notion of a cable-free digital sensor-bus was conceived using direct-write (DW) technology.

There are multiple DW methods commercially available ranging from plasma flame spray (PFS), to jetted atomized deposition (JAD) of nano-ink. The

basic principal remains the same; electrically conductive and insulative traces are selectively deposited with very fine tolerances either directly onto the structure or onto an intermediary substrate that can be applied onto the structure. As compared to a cable-based equivalent, the conformal DW traces essentially create a structural component with multifunctional capabilities, increasing instrumentation reliability while greatly reducing weight. Testing has shown DW traces to be extremely resilient to mechanical loading, and they can be designed impermeable to environmental factors with an epoxy encapsulant. Furthermore, this technology has already been demonstrated in a large scale production environment for aerospace applications for simple analog applications.

The present research further explores the use of DW technology as applied to a digital sensor-bus. A hypothetical SHM system of 100 digital sensor nodes distributed over a 100 m in total length was selected to benchmark an initial digital sensor-bus design. This paper describes the process whereby appropriate DW methods were selected, electrically conductive and insulative trace and layer dimensions were iteratively chosen, and an overall configuration was analytically optimized to achieve a digital sensor-bus design with the desired transmission characteristics. Finally, a proof-of-concept validation experiment is described.

2 SHM HARDWARE COMPATIBILITY

The overall goal of the present research was to take an existing SHM system that has proven reliable for detecting and characterizing damage in composites, and integrate it with DW methods to allow for cable-free power and data transmission. This section describes the SHM hardware necessary to accomplish this objective, as well as the system requirements for the DW sensor-bus to be compatible. Finally a discussion is presented for concept to physically integrate the SHM hardware with the sensor-bus.

2.1 Digitization

Present remote monitoring techniques utilize various sensors mounted in regions of interest, however quantity and location of these sensors are limited by the implied infrastructure. This includes wires for power and communication that run from each sensor to data acquisition units that can occupy large volumes to accommodate high sensor densities, as seen in Figure 1. To resolve these issues, the present investigators have patented the concept of point-of-measurement (POM™) digitization (US07373260). Essentially, by converting analog sensor output into digital signals at the local level, instrumentation can be minimized by enabling a serial bus configuration to transmit data.

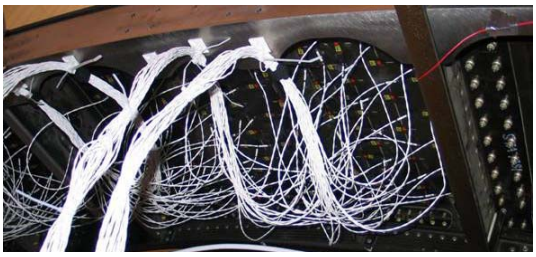

Figure 1: Example of SHM system wiring

Using this POM™ methodology, data volume can also be greatly reduced by locally implementing signal processing and feature extraction techniques. In this case, programmable logic can differentiate important data that needs to be reported to a central processor from status-quo information.

For the benchmark sensor-bus design, the Intelli-Connector™ digital SHM node, seen in Figure 2, was selected to achieve POM™ digitization. The Intelli-Connector™, developed by the present investigators, uses distributed acquisition as an alternative to traditional instrumentation, such as oscilloscopes and function generators. This system is also capable of local computation and processing. Designed mainly for piezoelectric-based methods that allow large-area coverage with reduced sensor densities, the Intelli-Connector™ can facilitate remote SHM for guided waves (GW), frequency response (FR) and acoustic emission (AE) techniques. The device is 25 mm diameter by 8 mm tall, weighs 4 g, and is encapsulated in urethane to conform to MIL-STD-810 and DO-160. The Intelli-Connector™ can excite arbitrary functions over 3.4 MS/s at 20 V_{pp}, and can digitize 16-bit data at 1 MHz with remotely programmable gains. Through various programs, this SHM node has been validated through a technology readiness level (TRL) of 6. Also taken into consideration was the next generation Intelli-Connector™ HS design with 50 MHz capabilities—presently at a rapidly maturing TRL of 3—since there would be an opportunity to allow the results of the DW sensor-bus design to affect the SHM node design for better integration compatibility.

Figure 2: Intelli-Connector™ digital SHM node

2.2 System Requirements

DW technology allows reliable transfer of electrical signals through patterned traces. For this unique architecture to be successful however, the trace geometry, spacing and overall configuration must be precisely designed. The first step in this process is to understand the system requirements. Overall 4 sets of traces and/or layers would need to be considered: communication, synchronization, power, shielding. Both the current Intelli-Connector™ and the future HS version communicate via a controller area network (CAN). CAN is a differential fixed-impedance protocol, meaning that is requires 2 parallel conductors (CAN-high & CAN-low) with an impedance between 100-130 Ohms. Similarly, both devices allow optional independent high-speed digital synchronization over a RS-422 protocol, also a differential fixed-impedance protocol requiring 2 parallel conductors (sync-high & sync-low) between 100-130 Ohms.

For power, both devices have a maximum current draw of 108 mA, however the HS version has a higher supply voltage of 28 V_{DC} (power & ground) and a standby current draw of 30 mA. For the benchmark system, assuming there would be 1 exciting node and no more than 6 sensing nodes at a time, the total current draw would be ~ 3.5 A. Therefore, nominally 6 parallel traces would be necessary for CAN, sync and power. In addition, to adhere to best practice shielding is necessary. Ideally, parallel shield traces would separate the 3 former pairs of traces. Also, since the pairs cannot be twisted with DW, a shield layer should surround the CAN and sync traces to properly couple the pairs and protect them against EMI.

2.3 Physical Connectivity

Once the SHM node requirements have been determined, the next important step was to determine the best method to physically connect this hardware with the DW sensor-bus being designed. Presently, a FireWire connector is used to connect the sensor to a cable harness. It was determined that a connector would not work well in the case of DW however. First, because creating 3-D via's is very difficult, second because the traces are very close together, and third because a break in impedance on the main sensor-bus trunk may cause communication reflections. Furthermore, connectors add weight and potentially a failure point. Another possibility that was considered was bonding the sensor and/or flex directly over the DW traces to make contract. This was ruled about because of alignment complexities, and also because of concerns that the traces may interfere with the SHM methods themselves in such close proximity.

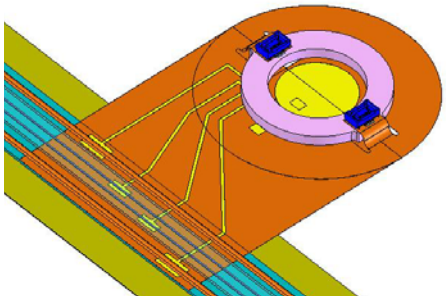

Figure 3: Schematic of SHM node flexible circuit w/tail

It was decided to make use of the flexible circuit that was already being employed on the bottom of the SHM node to connect the sensor elements to the digital board, and to extend a flexible "tail" outside the footprint of the sensor for the DW sensor-bus attachment, seen in Figure 3. This flex-tail would be bonded down to the structure, and would have a trace pattern identical to that of the DW bus (CAN, sync, power & shield), but using Kapton coverlay to selectively expose conductors at various points down its length. This flex-tail would be bonded down prior to the DW deposition stage, and the DW traces would be patterned directly over the conductors and then reinforced with an epoxy insulator (also part of the DW process). This will have the smallest mass impact, and should provide the most mechanically and electrically reliable and durable connection.

An experiment was performed in order to assure that this method would be successful. Two copper-coated Kapton flexible circuits were bonded to either end of a 2 composite plates, and parallel metallic traces were patterned over them using 2 DW prevalent methods: PFS (copper) and JAD (silver). The very positive results were a) nothing melted, b) the traces appeared to follow the layers without a problem, c) there was good electrical continuity, and d) there appeared to be no mechanical problems. The only negative result was that metallic power that was floating around during the PFS process stuck anywhere there was a gap, seam, or step on the composite plate. In most regions of the plate this powder could just be brushed or blown away, however at the interface with the flex circuit, this powder actually melted due to the close proximity of the PFS head, and formed a thin conductive path. This fused powder could not be easily cleaned, and shorted the parallel traces together, seen in Figure 4. This is not an insurmountable problem, but will need to be considered for the final design.

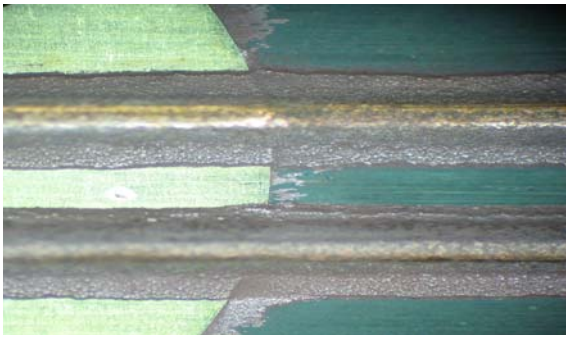

Figure 4: Shorted traces due to melted PFS powder

3 ELECTRICAL OPTIMIZATION

Physically connecting hardware to a DW sensor-bus is not sufficient to create an SHM-capable network. Communication and sync traces must match the prescribed impedance to daisy-chain multiple sensors on a common bus. Power lines must have enough area to carry the required current. Each of these traces must have low enough resistance to allow the signals to be carried along the desired total length for SHM coverage. Shield layers need to be sized to provide the desired protection without interfering with bus functionally. Thus, the next portion of research sought to measure the electrical properties of common DW materials, and collect a toolset of equations to be used for design optimization.

Again, the 2 main DW methods considered in this study are PFS and JAD. PFS typically uses copper as a conductor and can pattern traces from 0.3-1.5 mm wide (±50 μm) by 0.05-1mm thick (±10 μm) with a 2 mm pitch. JAD typically uses silver nano-particle ink as a conductor and can pattern traces from 0.1-0.3 mm wide (±5 μm) by 3-10 μm thick (±1 μm) with a 0.1 mm pitch. Both systems are compatible with various spray-on epoxy insulators.

3.1 Power Traces

The first set of traces investigated was for power. These traces were dominated by 3 factors: maximum voltage, maximum current and maximum total length. After inspection of the requirements, it was quickly determined that only PFS would meet the minimum geometry constraints. The following sub-sections describe the theories used to design the power traces, and the experiments used to validate these designs.

3.1.1 Voltage and current limitations

The first 2 problems were relatively simple geometric relationships; voltage carrying capacity is propositional to trace pitch, and current carrying capacity is proportional to trace cross-sectional area. The 2 documents that provide guidance on the design for current and voltage are MIL-STD-275E, "Printed Wiring for Electronic Equipment" and IPC-2221 "Generic Standard on Printed Board Design". From Table I in 4A of MIL-STD-275E and Table 6-1 in the IPC-2221 standard, the minimum trace spacing would be ~0.1 mm for up to 50 V_{DC} assuming a Type A5 assembly of external conductors with conformal coating. Similarly, from Figure 4A in MIL-STD-275E and Figure 6-4 in the IPC-2221 standard the minimum conductor cross sectional area to carry 3.5 A with a factor of safety of 2 would be 0.16 mm^2 assuming similar behavior to external etched copper conductors.

To validate these calculations for PFS, 3 sets of parallel copper traces with a 2.5 mm pitch were deposited on a 75 x 75 cm square graphite/epoxy plate in a meandering pattern with a total length of ~5 m, as seen in Figure 5. The first set measured slightly below the minimum theoretical area at ~0.1 mm^2, the second just above the minimum area at ~0.2 mm^2 and the third approximately twice the area at ~0.3 mm^2. A 40 V_{DC}, 15 A_{DC} power supply was connected to each pair of traces, and the current was measured with a multimeter. All sets of traces successfully carried 40 V_{DC} and 9.5 A_{DC} for over 5 minutes without any indication of failure.

3.1.2 Total length limitations

There is a limitation on total length of power traces for a given resistivity, because as the resistance gets too high, the voltage seen by the last node in the sensor-bus will drop below the 24 V threshold for excitation. To calculate the total allowable length, the SHM system was treated as a large circuit diagram. The 100 nodes were modeled as constant power dissipation sinks, with 93 consuming 0.8W while in standby, and 7 nodes consuming 3W while sensing. Each power trace between nodes was modeled as a small resister. Then, setting the input voltage to 28Vpp, Kirchhoff's laws could be used to solve for the maximum tolerable power trace resistivity. For the preliminary design, a node spacing of ½ m was selected, as well as copper traces with a conductivity equal to 58 x 10^6 S/m (IACS at 20°C). Using these assumptions, the equations dictated a minimum cross-sectional area of 1 mm^2.

Figure 5: Meandering PFS traces on a CFRP plate

To determine the conductivity of the PFS traces, the resistance of the traces and the geometry were measured from the plate described in Figure 5. The electrical conductivity is related to the trace resistance by $R=L / (\sigma * A)$ where R is the resistance, L is the trace length, A is the trace cross sectional area, and σ the electrical conductivity. Using this equation, the measured electrical conductivity averaged 17 x 10^6 S/m for the largest set of traces, 13 x 10^6 S/m for the middle set of traces and 8 x 10^6 S/m for the smallest set of traces. These values are low compared to the copper standard, with differences likely due to impurities, as well as geometry assumptions, since conductivity seems to decrease with increasing geometry. The consequence of this lower conductivity value is either a) fewer nodes can exist on the bus as designed, b) the nodes will need to be spaced closer together, or c) the traces will need to be re-sized.

3.2 Communication Traces

Several communication protocols were considered when this research commenced, including USB, Ethernet and FireWire. In the end, CAN was selected since a) it was relatively high-speed, b) it has a serial architecture, and c) it has a forgiving network topology. This last reason was the most critical; by allowing a range of impedance values from 100-130 Ohms, along with good error handling, CAN was the least sensitive to inconsistencies and tolerances for fabricated traces. CAN is governed by ISO 11898, is a mature protocol with more than 20 years of in-service applications, and is designed to allow devices to communicate without a host PC. It has a maximum transmission speed of 1 Mbit/sec for theoretically up to 2032 devices over 1,000 m, however practical limitations exist due to finite resistances, similar to those described in the prior section.

For CAN trace optimization, a Spice simulation model was constructed using the measured values for copper and the true CAN controller elements for each of the SHM nodes in the network. A single high/low CAN pulse pair was input into the traces on 1 end, and the differential voltage was displayed for the final node in the network. For digital communication, the key parameter is impedance. This value is a complex function of trace width, trace spacing, trace thickness, shield spacing, conductivity and dielectric constant for the insulation between the CAN traces and the shield layers.

Initial iterations determined that the required traces would need to be 0.25 mm by 10 μm thick with a 0.5 mm pitch. This of course is much finer than the PFS is capable of depositing, thus only JAD was considered for these traces. A plate identical to the one shown in Figure 5 was fabricated using JAD to measure the conductivity of the silver nano-ink particles. While this method was capable of achieving the required geometry, the measured resistance values were 3 orders of magnitude higher than desired for a 100 node system, approximately 1 kOhm per a 60 cm trace that should be less than 1 Ohm. The main issue is the extremely thin traces characteristic of present JAD techniques.

Therefore, while it is assumed that JAD methods will allow greater thickness traces in the near future, for the purposes of this research a screen printing process was developed for silver epoxy using chemical etched steel-shim templates. By using this method, much thicker silver traces can be patterned than with current JAD, and with finer pitch than PFS, just not with as much convenience as traditional DW methods. It was determined that the silver epoxy traces would need to be at least 125 μm thick, and therefore the model was updated to yield 0.33 mm wide traces with a 1.5 mm pitch. The synchronization traces would have an identical geometry as they also desire the same characteristic impedance range using RS-422.

3.3 Shield Traces

The shield layers mainly serve to protect the CAN and sync traces from electrical and mechanical interference (EMI), however digital traces are much less susceptible to noise than analog signals, particularly in differential mode. Guidelines show that even a minimal amount of metal, such as 1 μm, to be an excellent shield for digital signals against electrical interference up to 1MHz. Magnetic interference is much harder to transmit, but also much harder to protect against. Using 10 μm of metal would provide mild protection against magnetic interference up to 1MHz, however this layer would have to either get exponentially thicker or make use of a magnetic field absorbing material in order to provide better protection.

Beyond EMI, the shield layer can also play an important role in CAN impedance calculation. If in and out-of-plane shield layers are placed far enough away from the CAN traces, they have little influence. However, in a system being designed for minimum overall weight and cross-sectional area, everything must be as compact as possible. In this case, it was determined that so long as the in-plane shield traces have a pitch equal or greater to the CAN traces themselves, then they have negligible effect, thus this was how the design was specified. For the out-of-plane shields, they ended up playing a major role in the impedance within reasonable geometry, thus they were designed to be 0.5 mm above and below the CAN traces. The remaining volume between the CAN/sync and shield layers was filled with a dielectric material.

3.4 Electrical Insulation

The final element of the electrical design was the selection of the dielectric material to electrically isolate all of the conductors. PFS is compatible with a variety of ceramic insulators that offer good dielectric values, however they were not used mainly due to their stiffness not being compatible with SHM methods. JAD is compatible with several UV-curable epoxies that provide good stiffness, however pose manufacturing difficulties with curing thick sections.

Therefore, a simple spray-on epoxy method was devised to apply the electrically insulating layers in a cost-effective manner while still achieving the desired system characteristics. The requirements for material selection were a) dielectric constant of ~3 between 10 kHz and 1 MHz (ASTM D-150), b) service temperature of 250° C to survive a subsequent PFS process, c) a room temperature cure cycle to minimize the effect of mismatched thermal expansion coefficients, and d) a viscosity suitable for spraying. Multiple epoxies were procured that met these criteria at a range of viscosities for experimental validation of both the manufacturing process and their dielectric constant as measured by the ASTM. The actual dimensions of these insulating layers were completely dictated by the boundaries established conducting layer designs.

4 SHM METHOD COMPATIBILITY

The next major research effort aimed to investigate the effect of the DW bus on wave propagation. The main concern is that the presence of the DW traces would create GW scatter points, causing changes in signal phase and amplitude. To test this theory, 2 CFRP plates measuring 75 x 75 x 0.25 cm were instrumented with 3 pairs of PZT sensors bonded on opposite side of a pair of DW traces, as seen in Figure 6. The first plate used copper PFS traces representative of the designed power lines. Similarly, the second plate used JAD with representative of the CAN and sync lines. Pitch-catch and pulse-echo measurements were collected before and after the application of DW material.

Figure 6: Plate to evaluate SHM compatibility

4.1 Power Traces

The actuator and sensor pair used consisted of a concentrically placed lead zirconium titanate (PZT)-5A washer and disc. The actuator ring has outer and inner diameters of 0.5" and 0.29" respectively, while the sensor has a diameter of 0.25". Both have a thickness of 0.75 mm. In the "pulse-echo" mode the actuator is excited with a short time-span burst signal and the sensor in the same pair is used to sense Lamb-wave reflections caused by the burst from damage zones near the node. In "pitch-catch" mode, one or more sensors are used to record the response of the structure to excitation by an actuator at some distance in their vicinity.

4.1.1 Effect of PFS traces on GW signals

Baseline data for the panel was collected over a range of frequencies (50 to 500 kHz in steps of 50 kHz) before the traces were deposited. Subsequently, data was collected for the same range of frequencies after the PFS lines were applied. The signals were filtered using a zero-phase, high-order Butterworth filter to eliminate high and low frequency noise outside the excited bandwidth. This was followed by the Hilbert transform to extract the pitch-catch signal envelope.

A sample of the results is shown in Figure 7, specifically for the path between the 2 central sets of PZT. As seen in Figure 7, there is an observable difference in the pitch-catch signal transmitted across the power line. However, the difference is largely a result of some attenuation in signal amplitude rather than shape/phase. This is reflected in the values of the two metrics used to quantify this change, namely, the signal amplitude metric and the signal correlation metric. Both of these would be 100% if there was no change whatsoever between the two. The former is indicative of the combined amplitude and phase change, whereas the latter is insensitive to signal amplitude changes.

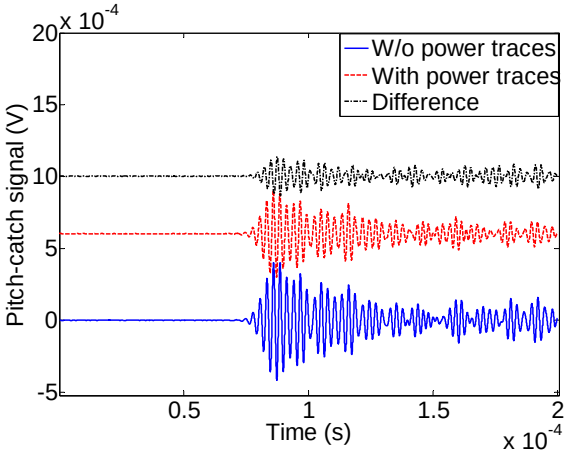

Figure 7: Pitch-catch with and without PFS

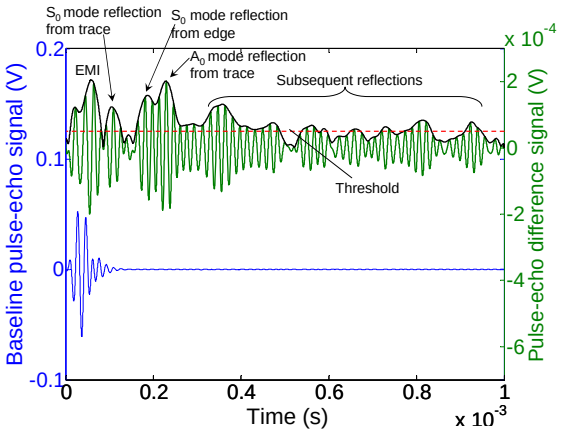

Figure 8: Pulse-echo difference for PFS traces

The average values of the two metrics across the path between the central 2 PZT pairs at the tested frequencies were tabulated. The larger drop in the amplitude metric (average of 26%) in comparison to the correlation metric (average of less than 2%) indicates that there is some attenuation in signal transmitted across the traces, but no significant change in signal shape. Similar trends were observed for the other pitch-catch paths.

The traces also cause a small but detectable reflection in pulse-echo signal when the difference between the signals taken before and after the deposition of the power traces is examined, shown in Figure 8. Based on these reflections (which consist of both possible modes, namely the zero-order symmetric (S0) and antisymmetric (A0) modes) the traces can be located relative to the nodes. For example, from the signals in Figure 8, and the wave speeds for the two modes at 50 kHz determined from the baseline pitch-catch signals, the location of the traces relative to PZT is 18.2 cm, which is 18 mm from the actual location. Thus, while there is some effect on the Lamb-wave signals, this is largely a wave attenuative effect and would not be expected to affect SHM performance.

4.1.2 Effect of PFS traces on SHM performance

To explicitly determine if the results from the previous sub-section would impact the ability to of this SHM method to detect damage in the presence of DW traces, a second set of experiments was performed using shear-gel coupled magnets to represent damage. Based on the initial tests, a lower frequency of 30 kHz was chosen. Multiple baseline pulse-echo signals were collected to examine signal repeatability for the panel (with the DW traces) and obtain a threshold value. The signal repeatability was not adversely affected and threshold values were consistent with those observed before the traces were deposited. A cylindrical magnet 12.7 mm diameter by 6 mm tall was placed first half-way between the sensor and the PFS traces, and then half-way between the PFS traces and the far sensor on the oppose side.

During first test, a clear reflection from the magnet is discernible above the threshold, as seen in Figure 9. At this lower frequency, the A0 mode dominates much more strongly than the S0 mode reflection, which is not discernible above the threshold. Based on the A0 mode reflection and using wavespeeds estimated from pitch-catch tests, the magnet's location was estimated to be 9.7 cm, which is 2.5 mm from the actual position. Based on this result and the amplitude of the pulse-echo difference signal over the threshold seen in Figure 9, the range of each node is estimated to be a circular region with radius of approximately 40 cm for this particular CFRP plate. Note that this estimate is independent of the presence of the power line trace, since the magnet is on the near side of the trace, relative to the node.

Next, to observe if damage can be detected by if located beyond the PFS traces, the magnet was placed in the second prescribed position. The signals from this test are shown in Figure 10, with a reflection from the magnet still appearing above the threshold value. Based on the A0 mode reflection, the magnet's location was estimated to be 31.2 cm, which is only 5 mm from the actual position. Thus, the range estimate of the nodes from the earlier test is justified. This range is also consistent with prior tests performed by the investigators on similar CFRP panels.

While there was some effect on the Lamb-wave signal amplitude due to the PFS traces on, when the signals before and after the DW process are compared, the signal shape is not significantly affected. In particular, the ability for this method to detect and localize damage was not compromised, confirmed by described test results using magnets to simulate damage. In addition, the range of this method from each PZT sensor was not significantly changed by the presence of the power line traces

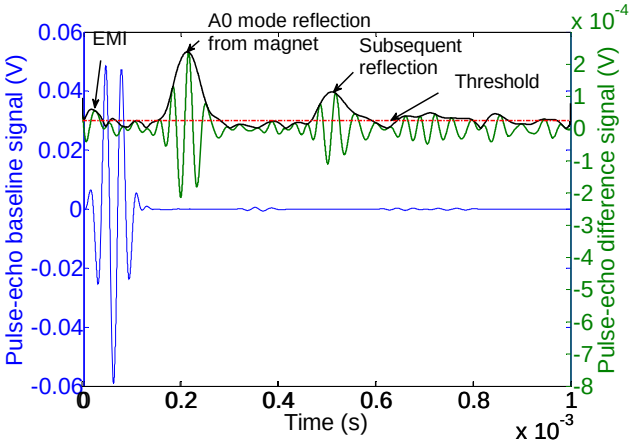

Figure 9: Pulse-echo with magnet in near position

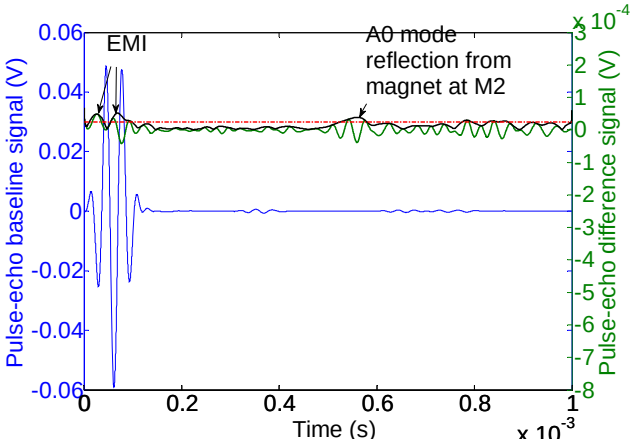

Figure 10: Pulse-echo with magnet in far position

4.2 Communication & Sync Traces

Once it was established that the power traces would not adversely affect the ability to detect damage, there was confidence that the other traces would have even less of an effect since they were all significantly smaller with less deposited material. Nevertheless, for completeness an identical test matrix was conducted for the JAD CAN and sync traces. Like the PFS pitch-catch tests, a difference was observed in comparing the response with and without the silver traces. In this case however, the amplitude metric had a much smaller change (average of 8.9%) and the correlation metric had nearly no change (average of 0.6%). Similar changes were observed for the pulse-echo results. From the pulse-echo response seen in Figure 11, and the wave speeds for the two modes at 50 kHz determined from the baseline pitch-catch signals, the location of the trace relative to the central PZT was 1.4 cm, which is 2.5 mm from the actual position.

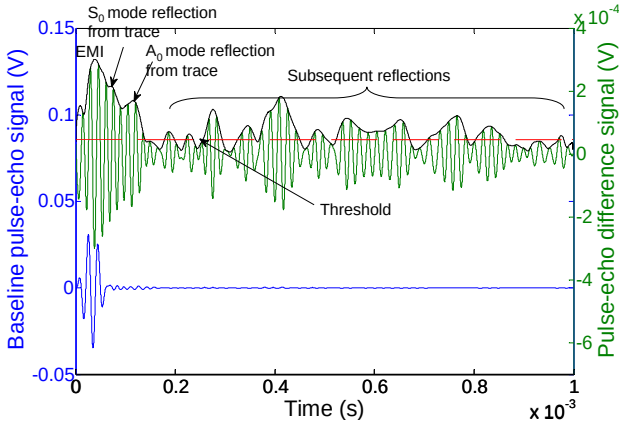

Figure 11: Pulse-echo difference for JAD traces

4.3 Mitigation Techniques

One reason why neither sets of traces may have had a large effect on the wave propagation is due to a mitigation technique that was employed by the investigators. From prior research it has been determined that placing a thin polymer layer (125 – 250 μm) under potential wave scattering points can be an effective means of decoupling these features from the propagation path. The combination of low stiffness compared to the plate structure, acoustic impedance mismatch, and damping properties of the polymer essentially "hide" the stiffness of other features bonded above as the wave travels underneath, so long as the layer is thick enough.

In this case, a 125 μm thick PEEK pressure sensitive adhesive (PSA) was selectively applied to the plate prior to the DW processes. The PSA also prevented the traces from shorting out on the conductive graphite fibers, and provides a moisture barrier for the composite material. Furthermore, this method could provide a simple path to removing the DW bus in the future if for some reason it needed to be repaired or replaced, as opposed to grinding it off of the structure.

5 SYSTEM INTEGRATION

One of the first conclusions of this research was that based on the present limitations of the PFS and JAD methods, it was evident that neither method would be able to be used exclusively to create a sensor-bus. PFS could be made thick enough for power traces but had too poor positional tolerances for communication lines, and JAD could be made accurately for controlled impedance, but only very thinly and thus not suitable to carry power. Clearly a hybrid approach is necessary. This section describes the overall configuration necessary to achieve the sensor-bus, integrating each of the individual element designs, as well as the required fabrication process. Furthermore, a planned proof-of-concept demonstration is described.

5.1 Overall Configuration

One of the great challenges of this digital sensor-bus development was the integration of all of the system elements into complete design. A balance had to be struck between maintaining the optimized component characteristics, and minimizing the overall bus geometry and mass, so as not to lose the original benefits of DW over traditional instrumentation. Furthermore, it was important to consider the manufacturing processes, described further in the following sub-section, so that this configuration would be able to be fabricated. The overall final configuration can be seen in Figure 12 (not to scale).

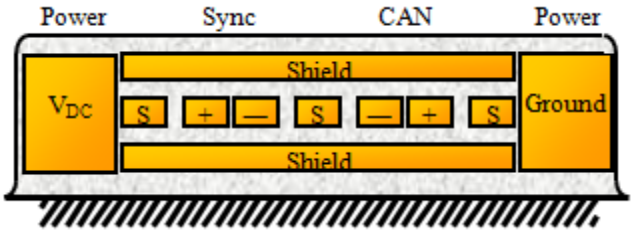

Figure 12: Schematic of final integrated configuration

From the design, each of the shield (S), CAN (+/-) and sync (+/-) traces would be 330 µm wide by 125 µm thick with a 1.5 mm pitch. Top and bottom shield layers of 10 µm thick would surround all of these traces with a 1 mm pitch. Epoxy would fill in the gaps between traces and layers to maintain their prescribed relative placement and provide electrical insulation. The power and ground traces would be placed on either side of the communication/sync stack, and would each be 1.25 mm wide by 0.4 mm thick, with a 12 mm effective pitch. Finally an encapsulant such as a urethane would be applied over the entire assembly. Overall dimensions end up being approximate 1.35 cm wide by 1.25 mm thick, and would weigh around 25 g per meter of length. Thus impact to the benchmark system would be 2.5 kg for the DW digital sensor-bus and ~1.5 kg for the new digital sensors themselves.

5.2 Manufacturing Process

To effectively achieve the overall configuration as described in the previous section, multiple DW and spray operations would need to be choreographed. The order of these operations would be important to maintain the desired geometry and not risk trace shorts. The manufacturing steps would include:

1. Apply PEEK PSA as a non-conductive layer along where the bus will be laid
2. Spray silver ink over PEEK as bottom shield (can also be pre-coated on PEEK)
3. Spray epoxy over silver using template to prescribed thickness (UV-curable easiest)
4. Bond sensors to structure with the flex-tails extending into the sensor-bus write region
5. JAD is used to pattern the CAN, sync & in-plane shield traces centered on the bus area
6. Spray epoxy to insulate JAD traces and build thickness for next layer (UV-curable)
7. Spray silver ink over epoxy as top shield, using a mask to contain the layer width
8. PFS is used to deposit power and ground traces on either side of the JAD
9. Spray urethane over entire assembly using template for desired shape
10. Remove all masks and clean area around sensor-bus for any copper dust

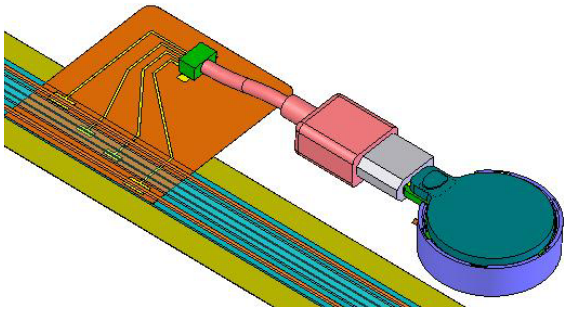

Figure 13: Schematic of initial implementation

5.3 Initial Implementation

For the initial implementation of this configuration and manufacturing process, there needed to be a few deviations from the production design to accommodate present resources. First, while the digital HS sensors will be directly compatible with the final design using the flex-tail to directly connect with the hardware, seen in Figure 3, for the proof-of-concept demonstration the existing SHM nodes will be used to better evaluate the digital sensor-bus itself with more mature nodes. In this case, since the original Intelli-Connector™ connects to power and CAN through a FireWire connector, it is not directly compatible with the designed DW bus. Therefore, an adapter was designed for the flex-tail, seen in Figure 13, where the original overwrite portion of the design remains the same, but rather than directly connecting into the digital node through a board connector, a small portion of FireWire cable is crimped into a reciprocal board connector that is then plugged into the SHM node. Secondly, since the current JAD process can only easily produce traces that are too thin for CAN lines, a silk-screen process was used here, filling in a chemical-etched steel shim with thick silver epoxy. Finally, since the silver traces were applied manually, only the CAN lines were laid down to demonstrate system functionality at lower risk.

5.4 Proof-of-Concept Demonstration

The final culmination of this research was to fabricate the initial implementation of this digital sensor-bus, as described in the previous sub-section, to demonstrate all the designs integrated together. A mask was chemical-etched from steel shim stock to expose a "U" shaped channel on a 75 x 75 x 0.25 cm CFRP plate. The modified manufacturing process from the previous 2 sub-sections was carried out, inserting 5 flex-tails, as seen in Figure 14. Intelli-Connector™ SHM nodes were bonded to the center of the plate in an isosceles triangle formation, and then plugged into the 3 flex-tail adapters in the middle of the sensor-bus. At the end of the bus a small CAN terminator plug was inserted to establish the correct line impedance for transmission.

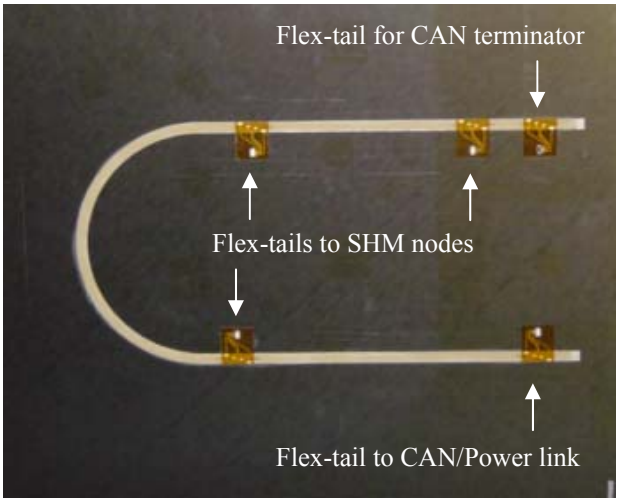

Figure 14: Picture of demonstration plate

This final demonstration sought to replicate a common experiment that has been performed by the present investigators numerous times on a variety of types of plates, however in this case the DW digital sensor-bus would be used for power and communication in place of the traditional FireWire cable harness. A small adapter was plugged into the front of the bus that converts the CAN signal to a USB protocol, which was then connected to a laptop to control the damage detection experiment. A cylindrical magnet (representing inverse damage due to increased local stiffness) 12.7 mm diameter by 6 mm tall was placed on the plate using shear-gel in various locations within the triangle formed by the SHM nodes (similar to the SHM feasibility experiments reported in an earlier section). From the PC control, Lamb-wave pulse-echo tests were commanded for each of the SHM nodes, and their response was stored in comma-delimited files on the PC.

Subsequently, a Matlab™ algorithm was executed to predict the location of the magnet based on the nearest intersection of the damage radii estimates from each of the SHM nodes. Following this procedure 10 times without and 10 times with the magnet in different positions, no communication or power problems were encountered and the presence of the magnet was correctly identified each time. Across these trials, the average error in the distance predicted by the algorithm was 7.5 mm.

6 CONCLUSION

This paper explores the novel application of direct-write (DW) techniques to create a digital sensor-bus for structural health monitoring (SHM) applications. A benchmark system of 100 digital SHM nodes over a 100 m was defined, and system hardware requirements for communication and power were determined. Using these specifications, trace material, fabrication process and geometry were determined for CAN, sync, power and shield. Subsequently an experimental procedure was followed to evaluate the electrical properties of DW traces to be used within the models, and Lamb waves were used to evaluate the impact of DW traces on existing damage detection algorithms. Finally, a design to physically connect the DW digital sensor-bus to existing and next generation SHM nodes was devised and demonstrated through a proof-of-concept damage localization experiment.

Overall this research was considered very successful in achieving its goal of demonstrating a DW digital sensor bus for SHM applications that does not impact the ability to detect damage. Both DW methods considered in this research suffer from relatively high resistivity, which until resolved, may limit the total length of bus that can be deployed. Future work will aim to seek lower-resistance solutions through improved materials and refined processes. The authors also plan to use video alignment tools to improve DW placement accuracy, and investigate DW for creating electrodes on carbon nano-tube (CNT) enhanced composite materials for in-situ SHM.

ACKNOWLEDGMENT

Research regarding the development of a direct-write digital sensor-bus was sponsored by NASA Ames Research Center, under the Phase I SBIR contract NND09CC57P. Work was performed at Metis Design Corporation in Cambridge, MA in collaboration with The Boeing Corporation in Seattle, WA, St. Louis, MO and Mesa, AZ.

Research regarding the development of point-of-measurement digitizing SHM sensors was sponsored by Air Force Office of Scientific Research, under the Phase II SBIR contract FA9550-05-C-0024. Work was performed at Metis Design Corporation in Cambridge, MA in collaboration with the Massachusetts Institute of Technology in Cambridge, MA.

Research regarding the development of a high-speed direct-write compatible SHM sensor was sponsored by Air Force Research Laboratory Air Vehicle Directorate, under the Phase II SBIR contract FA8650-08-C-3860. Work was performed at Metis Design Corporation in Cambridge.

Research regarding the integration of direct-write with CNT-enhanced composite laminates for SHM was sponsored by Air Force Office of Scientific Research, under the Phase I SBIR contract FA9550-09-C-0165. Work was performed at Metis Design Corporation in Cambridge, MA in collaboration with the Massachusetts Institute of Technology in Cambridge, MA.

REFERENCES

(Chang, 1999) F. Chang. "Structural Health Monitoring: A Summary Report." *Proceedings of the 2nd International Workshop on Structural Health Monitoring*, Stanford, CA, 1999.

(Neumair, 1998) M. Neumair. "Requirements on Future Structural Health Monitoring Systems." *Proceedings of the 7thRTO Mtg*. 1998.

(Hall, 1999) S. Hall. "The Total Data Integrity Initiative—Structural Health Monitoring, The Next Generation." Proceedings of the USAF ASIP. 1999.

(Van Way, 1995) C. Van Way, J. Kudva.and J. Schoess. "Aircraft Structural Health Monitring System Development—overview of the Air Force/Navy Smart Structures Program." *Proceedings of the SPIE Symposium on Smart Structures, San Diego*, CA. 1995.

(Derriso, 2007) M Derriso, S.Olson, M. Desimio and D.Pratt."Why Are There Few Fielded SHM Systems for Aerospace Structures?" Proceedings of the 6th International Workshop on SHM, Stanford University. 2007.

(MIL, 2007).MIL-STD-461F "Requirements For The Control Of Electromagnetic Interference Characteristics Of Subsystems And Equipment." United States Department of Defense. 2007.

(MIL, 1984) MIL-STD-275E. "Printed Wiring For Electronic Equipment" United States Department of Defense. 1984.

(RTCA, 2007) RTCA/DO-160F. "Environmental Conditions And Test Procedures For Airborne Equipment" Radio Technical Commission for Aeronautics. 2007.

(IPC, 1998). IPC 2221. "Generic Standard on Printed Board Design" Institute for Interconnecting and Packaging Electronic Circuits. 1998.

(FAA, 2005) FAA-G-2100H. "Electronic Equipment, General Requirements" Federal Aviation Administration. 2005

(ANSI, 2005). ANSI-422-B. "Electrical Characteristics of Balanced Voltage Digital Interface Circuits" American National Standards Institute. 2005.

(FAR,2008) Title 47.15. "Code of Federal Regulations" Federal Communication Commission. 2008.

(ISO, 2006) ISO 11898. "Road Vehicles -- Controller Area Network (CAN)", International Organization for Standardization, Geneva, Switzerland. 2006.

(Voss, 2005) W. Voss. *A Comprehensible Guide To Controller Area Network*, Copperhill Technologies Corp., Greenfield, MA, pgs 17, 133-139. 2005.

(Ott, 1998) W. Ott. *Noise Reduction Techniques in Electronic System.*, Wiley-Interscience, New York, pg 201-495. 1998.

(Wadell, 1991) B. Wadell. *Transmission Line Design Handbook.* Artech House, Boston, pg 231-232. 1991

(Johnsone, 2008)H. Johnsone and M. Graham. (2008). *High-Speed Signal Propagation, Advanced Black Magic.* Prentice Hall PTR, Upper Saddle River, pg 382. 2008

(TI, 2009) TI SN65HVD23X 3.3-V CAN Transceiver. Texas Instruments. 2009

(Lamb 1917) H. Lamb. "On Waves in an Elastic Plate." Proceedings of the Royal Society of London, Part A: Containing Papers of a Mathematical and Physical Character, v.93, n.651, pgs 293-312. 1917.

(Viktorov 1967) I. Viktorov. *Rayleigh and Lamb Waves*, Physical Theor. Plenum Press, New York. 1967.

(Nayfeh, 1995) A. Nayfeh. *Wave Propagation in Layered Anisotropic Media*. v.39, Elsevier, Amsterdam. 1995.

(Dalton, 2001) R. Dalton, .P. Cawley and M. Lowe. "The potential of Guided Waves for Monitoring Large Areas of Metallic Aircraft Fuselage Structure." *Journal of Nondestructive Evaluation*, v.20, pgs 29-46. 2001.

(Kessler, 2002) S. Kessler, S Spearing and C. Soutis. "SHM in Composite Materials using Lamb Wave Methods." *Smart Materials and Structures*, v.11, 269-278. 2002.

(Raghavan, 2007) A. Raghavan and C. Cesnik. "Review of Guided-Wave SHM," *The Shock and Vibration Digest*, v. 39, p. 91-114. 2007.

(Kessler, 2006) S. Kessler, C. Dunn, J. Chambers and B. Wardle. "Intelligent Multi-Sensing SHM" AFOSR final report FA9550-05-C-0024. 2006.

(Kessler, 2009) S. Kessler and A. Raghavan. "Vector-based Damage Localization for Anisotropic Composite Laminates." Proceedings of the 7th International Workshop on Structural Health Monitoring, Stanford University. 2009.

(Dunn, 2009) C. Dunn, A. Raghavan and S. Kessler. "Analytical Axisymmetric Coupled Piezo-Elastodynamic Models for Guided-Wave Structural Health Monitoring." Proceedings of the 7th International Workshop on Structural Health Monitoring, Stanford University. 2009.

(Raghavan, 2009) A. Raghavan., S. Kessler, C. Dunn, D. Barber, S. Wicks and B. Wardle. "Structural Health Monitoring using Carbon Nanotube (CNT) Enhanced Composites." Proceedings of the 7th International Workshop on Structural Health Monitoring, Stanford University. 2009.

(Barber, 2009) D. Barber, S. Wicks, B. Wardle, A. Raghavan, C. Dunn and S. Kessler."Health Monitoring of Aligned Carbon Nanotube (CNT) Enhanced Composites." Proceedings of the SAMPE Fall Technical Conference, Wichita, KS. 2009.